A 3D Ad Hoc Localization System using Aerial Sensor Nodes

Euiho Kim and Dongkyu Choi, *Member, IEEE*

***Abstract*—An ad hoc localization system (AHLoS) is necessary at a time or place where Global Satellite Navigation Systems are not available and a permanent infrastructure is not needed. Previous work on such systems has typically focused on 2D horizontal navigation, but new applications such as those for Unmanned Aerial Systems (UAS) require a 3D navigation capability. In this paper, we present an AHLoS utilizing aerial nodes in the form of quadrotors or similar platforms in addition to fixed, ground-based nodes to provide a precise 3D positioning capability. The nodes are equipped with Ultra Wide Band devices to be used as ranging sources. Our mathematical analysis and simulated results suggest that the 3D AHLoS is capable of providing high positioning accuracy, most notably, the vertical accuracy that is better than a couple of decimeters for 95 percent of the time, making it ideal for various UAS applications.**

***Index Terms*—Ad Hoc Localization, 3D positioning, Global Positioning System, TDOA, TOA**

I. Introduction

THE Global Navigation Satellite Systems (GNSS) such as the Global Positioning System (GPS) provide reliable and accurate positioning in many applications including automobile navigation and aircraft landing. However, there are places where these systems become unreliable due to various reasons. For instance, the relatively low-power signal from GNSS does not reach indoor environments in a reliable manner, rendering its use infeasible. Furthermore, in remote areas like the polar regions, GNSS suffer from excessive ionospheric effects and noise due to low satellite elevation angles [1]. The signal is also susceptible to intentional or unintentional interferences hindering reliable positioning.

For these reasons, recent research explored the use of Wi-Fi, TV signals, and Ultra Wide Band (UWB) in place of GNSS [2]–[4]. In densely populated areas, some of these signals would be readily available in many places or could be added with relative ease. However, this is not the case in remote areas like the polar regions, and it can often be impractical to install permanent infrastructure in such areas, despite the scientific and military needs for a reliable alternative to GNSS. There, an Ad Hoc Localization System (AHLoS) can serve the needs with relatively small investments necessary.

There are several previous research on AHLoS. Reference [5] introduced an AHLoS that consists of unknown sensor nodes and a limited set of anchors. The anchors were assumed to know their global locations through GPS or manual configuration and served as ranging sources to the sensor nodes. The sensor nodes estimate their locations using the anchors through Time Difference of Arrival (TDOA) formulation and they themselves become anchors for the remaining sensor nodes.

Reference [6] proposed a similar AHLoS for 3D positioning, but it did not include any anchors with known global coordinates. Rather, their AHLoS sets up a local coordinate system using a few sensor nodes that were used as baseline anchors in the coordinate system.

Reference [7] introduces an AHLoS localization method based on angle of arrival (AOA) that provides the orientation and the position with a small number of anchors. For this method, each node must have AOA capability.

In all of the above three methods, the best fit of triangulation or multilateration in a least-squares sense was used to compute node and user positions. In contrast, the AHLoS in [8]–[10] used a semi-definite programming to solve the localization problem.

In this paper, we propose an AHLoS that is similar to [5] and [6] in the sense that: 1) a local coordinate system is set up using sensor nodes; and 2) the sensor nodes with initially unknown positions become anchors when their locations are found. Our novel contribution in the current work is the fact that we leverage aerial nodes equipped with UWB devices to provide more precise 3D positioning capability. The aerial nodes are in the form of quadrotors or similar platforms with reliable hovering capability. Our proposed AHLoS can be used as an alternative to or a back-up for GNSS.

This paper focuses on the feasibility assessment of the proposed AHLoS and the analysis of user positioning performance. In section II, we describe the deployment procedure for our 3D AHLoS which includes the set up of a local Cartesian coordinate system and aerial node localizations. Section III discusses the parameterization of user positioning performance and the effect of disturbances on the aerial node caused by wind, gust, or control errors. Section IV provides some simulation results and analyses before we conclude in Section V.

II. Deployment of 3D AHLoS Sensor Network

We construct our AHLoS in two steps. First, we define a local coordinate system based on the sensor node geometry on the ground [11], [12]. Next, we estimate the position of the sensor nodes on the ground and in the air through communication and range measurements [5], [13]. In this section, we describe each of these steps in detail.

E. Kim is with the Department of Aerospace Engineering, University of Kansas, Lawerence, KS, 66045 USA. E-mail: euiho.kim@ku.edu

D. Choi is with the Department of Aerospace Engineering, University of Kansas, Lawerence, KS, 66045 USA. E-mail: dongkyuc@ku.edu.

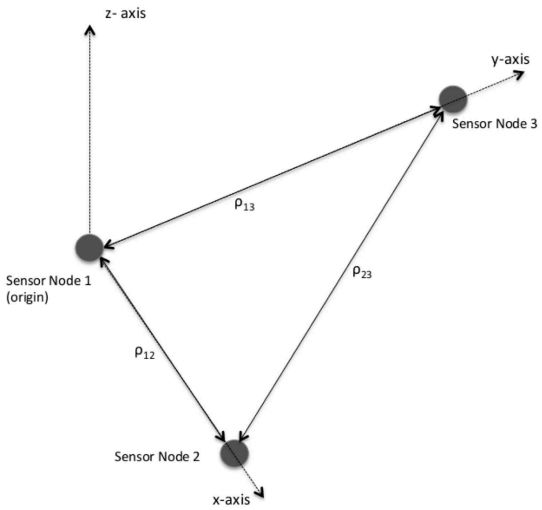

Fig. 1. Local cartesian coordinate system.

A. Local Coordinate System Determination Using Sensor Nodes On the Ground

Our localization system has both ground and aerial sensor nodes. To establish a coordinate system for the AHLoS, we use the sensor nodes on the ground that are assumed to be fixed. We assume that the sensor nodes use UWB pulses to measure distance among them using the Time of Arrival (TOA) of the pulses. Then we construct the local coordinate system as follows. First, the reference origin is set by placing the first sensor node, $\boldsymbol{s}_1$, at an arbitrary location $(s_{1,x}, s_{1,y}, s_{1,z})$ in the absolute coordinate system. The local coordinates of $\boldsymbol{s}_1$ is $(0, 0, 0)$ by definition. Second, the $\boldsymbol{x}$ axis of the local coordinate system is determined by the straight line from the first sensor node to the second sensor node as shown in Fig. 1. The local coordinates of the second sensor node, $\boldsymbol{s}_2$, is then $(\rho_{12}, 0, 0)$, where ρ_{12} is the range between the first and the second sensor nodes measured by the TOA between them. Third, the $\boldsymbol{y}$ axis of the local coordinate system is determined by placing the third sensor node, $\boldsymbol{s}_3$, so that the line between the first and the third nodes is perpendicular to the $\boldsymbol{x}$ axis as shown in Fig. 1. We can achieve this using the TOA measurements at $\boldsymbol{s}_3$ formulated as follows:

$$\begin{aligned} \rho_{13}^2 &= (s_{3,x} - s_{1,x})^2 + (s_{3,y} - s_{1,y})^2 \\ \rho_{23}^2 &= (s_{3,x} - s_{2,x})^2 + (s_{3,y} - s_{2,y})^2 \end{aligned} \tag{1}$$

From the perturbation linearization method [14], Eq. (1) is linearized at $\tilde{\boldsymbol{s}}_3$ which is closely located near $\boldsymbol{s_3}$

$$\underbrace{\begin{bmatrix} \delta\rho_{13} \\ \delta\rho_{23} \end{bmatrix}}_{\delta\boldsymbol{\rho}} = \underbrace{\begin{bmatrix} \frac{\tilde{s}_{3,x} - s_{1,x}}{\tilde{\rho}_{13}} & \frac{\tilde{s}_{3,y} - s_{1,y}}{\tilde{\rho}_{13}} \\ \frac{\tilde{s}_{3,x} - s_{2,x}}{\tilde{\rho}_{23}} & \frac{\tilde{s}_{3,y} - s_{2,y}}{\tilde{\rho}_{23}} \end{bmatrix}}_{G} \underbrace{\begin{bmatrix} \delta s_{3,x} \\ \delta s_{3,y} \end{bmatrix}}_{\delta\boldsymbol{s}} \tag{2}$$

where $\tilde{\boldsymbol{\rho}} = \boldsymbol{\rho} + \delta\boldsymbol{\rho}$ and $\tilde{\boldsymbol{s}} = \boldsymbol{s} + \delta\boldsymbol{s}$. Then, Eq. (2) is solved by

$$\delta\hat{\boldsymbol{s}} = G^{-1}\delta\boldsymbol{\rho} \tag{3}$$

The solution $\delta\hat{\boldsymbol{s}}$ is used to correct the initial guess of $\boldsymbol{s}_3$. Then, Eq. (2) and Eq. (3) are iteratively solved until the magnitude of $\delta\boldsymbol{\rho}$ becomes very small. Using this technique, the sensor node 3 can be placed where $\boldsymbol{s}_3 = (0, \rho_{13}, 0)$.

The coordinates of $\boldsymbol{s}_2$ and $\boldsymbol{s}_3$ are subject to some errors because their location is determined from distance measurements. Assuming that the error characteristics of the range measurement are Gaussian white noise, the errors in the coordinates of $\boldsymbol{s}_2$ and $\boldsymbol{s}_3$ would be significantly suppressed when a large sample measurements are averaged.

Finally, $\boldsymbol{z}$ axis is correspondingly determined to be perpendicular to the plane of $\boldsymbol{x}$ and $\boldsymbol{y}$ axes with right hand rules as shown in Fig 1. Based on this local coordinate system, we can add an arbitrary number of ground sensor nodes with minimal error in their positions.

B. Aerial Nodes Deployment and Localization

The sensor nodes placed on the ground according to the previous section can be used for 2D horizontal positioning. To form a reliable 3D AHLoS network, however, the system requires additional nodes with some vertical deviation from the ground. In our system, aerial nodes serve this purpose. We deploy these nodes according to some desired sensor node geometry.

The first aerial node must find its position using only the ground sensor nodes. For that to happen, the following two conditions should be satisfied for a reliable localization. First, it has been found from our initial simulations that at least four sensor nodes would be required on the ground with a reasonable geometry. In general, the range measurements from three sensor nodes with little vertical geometric difference are not likely to yield a converged or correct solution for the localization of the first aerial node.

Second, the initial guess of an aerial node position in Eq. (2) should have a positive height to prevent an incorrectly converged position below the ground due to the vertical ambiguity shown in Fig. 2. As shown, the aerial node and its mirror image below the ground can have the same range measurements. Depending on the initial condition of Eq. (2), the TOA solution may either converge toward the true position of the aerial node or its mirror image.

Once the first aerial node successfully reaches to its designated node position and starts acting as a ranging source, namely, as an anchor, the second aerial node uses the first aerial node as well as the ground nodes to estimate its position. The second node would likely have a more accurate position than the first aerial node due to the better anchor geometry. In turn, the second aerial node joins all the previous sensor nodes as an anchor.

Subsequently, the rest of the aerial nodes acquire their position information and become an anchor in a similar manner. When all of the aerial nodes become anchors, the system maintains the overall geometry through controlled hovering of all the aerial nodes. In this stage, the nodes continuously refine their positions by following a localization technique called *successive refinement* [13]. The aerial nodes sequentially measure their current position using all of the

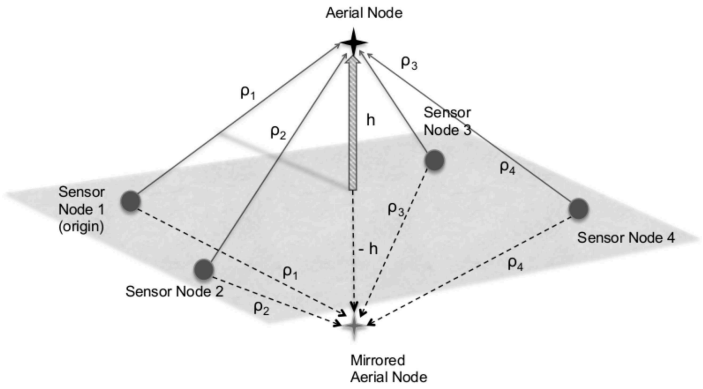

Fig. 2. The aerial node and its mirror image have the same range measurements from the sensor nodes on the ground.

available anchors and broadcast their updated coordinates. This process continues until the computed positions of all aerial nodes converge. The successive refinement is a cooperative positioning method and quickly lowers the variance of the positioning error. We analyze the convergence of the successive refinement mathematically in the next section.

C. Convergence of Successive Refinement

For generality, let us assume that there are n sensor nodes on the ground and denote them as *reference sensor nodes*. The first sensor node above ground, $\boldsymbol{s}_{air,1}$, estimates its position by using TOA measurements from the reference sensor nodes and has the following position variance

$$\sigma^2_{p,\boldsymbol{s}_{air,1}} = \text{trace}(G^\top_{R_1} W_R G_{R_1})^{-1} \tag{4}$$

where G_{R_1} is the 3D geometry matrix of $\boldsymbol{s}_{air,1}$ expanded from Eq. (2). W_R is the weighting matrix defined as

$$W_R = \begin{bmatrix} \frac{1}{\sigma^2_{R_1}} & 0 & \cdots & 0 \\ 0 & \frac{1}{\sigma^2_{R_2}} & & \\ \vdots & & \ddots & \\ 0 & \cdots & & \frac{1}{\sigma^2_{R_n}} \end{bmatrix} \tag{5}$$

where σ_{R_i} is the standard deviation of the range measurement using the i^{th} reference sensor node. For the reference sensor nodes, it is reasonable to assume $\sigma_{R_i} = \sigma_r$ for all i's where σ_r is the standard deviation of the range measurements noise that is modeled as Gaussian white noise.

Now, the second sensor node in the air, $\boldsymbol{s}_{air,2}$, can use $\boldsymbol{s}_{air,1}$ in addition to the n reference sensor nodes as ranging sources. The 3D rms spherical range uncertainty using $\boldsymbol{s}_{air,1}$ consists of the position error in Eq. (4) and the range measurement noise of σ_r as follows:

$$\sigma^2_{\boldsymbol{s}_{air,1}} = \sigma^2_{p,\boldsymbol{s}_{air,1}} + \sigma^2_r \tag{6}$$

Hence, its positioning uncertainty of $\boldsymbol{s}_{air,2}$ is

$$\begin{aligned} \sigma^2_{p,\boldsymbol{s}_{air,2}} &= \text{trace}\left(\begin{bmatrix} G_{R_2} \\ G_{s_{air,1}} \end{bmatrix}^\top \begin{bmatrix} W_R & 0 \\ 0 & \frac{1}{\sigma^2_{\boldsymbol{s}_{air,1}}} \end{bmatrix} \begin{bmatrix} G_{R_2} \\ G_{s_{air,1}} \end{bmatrix} \right)^{-1} \\ &= \text{trace}\left(\begin{bmatrix} G_{R_2} \\ G_{s_{air,1}} \end{bmatrix}^\top \begin{bmatrix} W_R G_{R_2} \\ \frac{G_{s_{air,1}}}{\sigma^2_{\boldsymbol{s}_{air,1}}} \end{bmatrix} \right)^{-1} \\ &= \text{trace}\left(G^\top_{R_2} W_R G_{R_2} + \frac{1}{\sigma^2_{\boldsymbol{s}_{air,1}}} G^\top_{s_{air,1}} G_{s_{air,1}} \right)^{-1} \end{aligned} \tag{7}$$

where $G_{s_{air,1}}$ is the geometry matrix of $\boldsymbol{s}_{air,1}$ viewed from $\boldsymbol{s}_{air,2}$.

Once the position of $\boldsymbol{s}_{air,2}$ is available, the position estimate of $\boldsymbol{s}_{air,1}$ can, in turn, be improved and has a similar uncertainty to Eq. (7)

$$[\sigma^2_{p,\boldsymbol{s}_{air,1}}]_1 = \text{trace}\left(\underbrace{G^\top_{R_1} W_R G_{R_1}}_{A} + \underbrace{\frac{1}{\sigma^2_{\boldsymbol{s}_{air,2}}} G^\top_{s_{air,2}} G_{s_{air,2}}}_{B} \right)^{-1} \tag{8}$$

where $[\sigma^2_\cdot]_k$ denotes the variance from the k^{th} iteration. $G_{s_{air,2}}$ is the geometry matrix of $\boldsymbol{s}_{air,2}$ viewed from $\boldsymbol{s}_{air,1}$.

In Eq. (8), A and B are covariance matrices whose characteristics are real symmetric and non-negative definite. If we let $\lambda(\cdot)$ denote the eigenvalue of a matrix, the following eigenvalue inequality holds [15]

$$\lambda(A+B)_i \geq \lambda(A)_i, \text{ for } i = 1, 2, \cdots, m \tag{9}$$

and $\lambda_1 \geq \lambda_2 \geq \cdots \geq \lambda_m$. When $A+B$ and A are invertible, their eigenvalues are bigger than zero. In this case, note that

$$\begin{aligned} \text{trace}(A+B) &= \sum_i^m \lambda(A+B)_i \\ &\geq \text{trace}(A) \\ &= \sum_i^m \lambda(A)_i \end{aligned} \tag{10}$$

and

$$\begin{aligned} \text{trace}(A+B)^{-1} &= \sum_i^m \frac{1}{\lambda(A+B)_i} \\ &\leq \text{trace}(A)^{-1} \\ &= \sum_i^m \frac{1}{\lambda(A)_i} \end{aligned} \tag{11}$$

Therefore, Eq. (4) and Eq. (8) result in the following relationship:

$$[\sigma^2_{p,\boldsymbol{s}_{air,1}}]_1 \leq \sigma^2_{p,\boldsymbol{s}_{air,1}} \tag{12}$$

Now, $\boldsymbol{s}_{air,2}$ updates its position using the improved $[\sigma^2_{\boldsymbol{s}_{air,1}}]_1 = [\sigma^2_{p,\boldsymbol{s}_{air,1}}]_1 + \sigma^2_r$ instead of $\sigma^2_{\boldsymbol{s}_{air,1}}$. Then the

position variance of $\boldsymbol{s}_{air,2}$ is

$$\begin{aligned}[\sigma^2_{p,\boldsymbol{s}_{air,2}}]_1 &= \text{trace}\Bigg(G_{R_2}^\top W_R G_{R_2} \\ &\quad + \frac{1}{[\sigma^2_{\boldsymbol{s}_{air,1}}]_1} G^\top_{s_{air,1}} G_{s_{air,1}} \Bigg)^{-1} \\ &= \text{trace}\Bigg(\underbrace{G_{R_2}^\top W_R G_{R_2} + \frac{1}{\sigma^2_{\boldsymbol{s}_{air,1}}} G^\top_{s_{air,1}} G_{s_{air,1}}}_{A'} \\ &\quad + \underbrace{\left(\frac{1}{[\sigma^2_{\boldsymbol{s}_{air,1}}]_1} - \frac{1}{\sigma^2_{\boldsymbol{s}_{air,1}}} \right) G^\top_{s_{air,1}} G_{s_{air,1}}}_{B'} \Bigg)^{-1} \quad (13)\end{aligned}$$

Likewise, A' and B' in Eq (13) are real symmetric and non-negative definite matrices. Assuming the matrices $A' + B'$ and A' are invertible, the iterated $[\boldsymbol{s}_{air,2}]_1$ has the following relationship from Eq. (9):

$$[\sigma^2_{\boldsymbol{s}_{air,2}}]_1 \leq \sigma^2_{\boldsymbol{s}_{air,2}} \quad (14)$$

As the number of iteration increases, $[\sigma^2_{\boldsymbol{s}_{air,1}}]$ and $[\sigma^2_{\boldsymbol{s}_{air,2}}]$ will become lower and converge to some values. The convergence of them is also shown through simulation later in this paper.

III. User Positioning Performance

Once all the sensor nodes are deployed and their localization is complete with converged solutions through successive refinements, they can act as ranging sources to provide position information to users. One possible positioning framework is to have the sensor nodes time-synchronized and to transmit UWB ranging pulse signals at the same time, which is similar to what the GPS employs. Each node position is delivered to the user embedded in the ranging pulses as messages. Then, a user is able to compute its position using a Time Difference of Arrival (TDOA) formulation. In this method, however, Time-Hopping Spread Spectrum or Direct-Sequence Spread Spectrum must be implemented in the UWB system to minimize the multiple access interference between nodes [16].

An alternative approach is where a user transmits a UWB pulse to the anchors that are time-synchronized. In this framework, there is a master station or anchor that gathers the time stamps of the received signals from each anchor and computes the user position. Then the master station sends back the computed position to the user. Avoiding transmitting UWB pulses at the same time, this architecture could be less susceptible to the multiple access interference. However, the delivered user position from the master station has a time delay and needs to be further processed for a user with high dynamics. This paper uses the former approach as a positioning architecture.

This section first reviews the parameterization of the TDOA positioning accuracy. Then, the effect on the user positioning performance from the possible aerial node disturbances will be discussed.

A. TDOA Positioning Accuracy

There are several error sources in the TDOA positioning system. The main error sources include the time synchronization between sensors, noise in range measurements, and deviation in sensor coordinates. In combination, they cause range measurement errors that are translated into user positioning errors via a user-to-ranging-source geometry.

To analyze such errors, let us assume that there are m measurements from the sensor nodes. The origin of the local coordinate is located at the reference sensor node 1, $\boldsymbol{s}_1$. Then, a TDOA equation at user location, $\boldsymbol{x}_u$, can be formulated as

$$c\Delta\boldsymbol{t} = f(\boldsymbol{s}, \boldsymbol{x}_u) = \begin{bmatrix} \|\boldsymbol{x}_u - \boldsymbol{s}_2\| - \|\boldsymbol{x}_u - \boldsymbol{s}_1\| \\ \|\boldsymbol{x}_u - \boldsymbol{s}_3\| - \|\boldsymbol{x}_u - \boldsymbol{s}_1\| \\ \vdots \\ \|\boldsymbol{x}_u - \boldsymbol{s}_m\| - \|\boldsymbol{x}_u - \boldsymbol{s}_1\| \end{bmatrix} \quad (15)$$

where c is the speed of light.

Eq. (15) can be solved by using a taylor series expansion through iteration. Assuming that $\tilde{\boldsymbol{x}}_u$ is close to $\boldsymbol{x}_u$, then the taylor expansion of Eq. (15) is

$$c\Delta\boldsymbol{t} = f(\boldsymbol{s}, \boldsymbol{x}_u) = f(\boldsymbol{s}, \tilde{\boldsymbol{x}}_u) + \frac{\partial f(\boldsymbol{s}, \tilde{\boldsymbol{x}}_u)}{\partial \boldsymbol{x}_u} \delta \boldsymbol{x_u} + H.O.T \quad (16)$$

Ignoring $H.O.T$ in Eq. (16) and denoting the partial derivatives as H, the difference between $\tilde{\boldsymbol{x}}_u$ and $\boldsymbol{x}_u$, i.e. $\delta\boldsymbol{x}_u$, can be estimated by solving

$$\delta\hat{\boldsymbol{x}}_u = (H^\top W H)^{-1} H^\top W (c\Delta\boldsymbol{t} - f(\boldsymbol{s}, \tilde{\boldsymbol{x}}_u)) \quad (17)$$

where W is the TDOA weighting matrix incorporating ranging accuracies. The gradient matrix $\boldsymbol{H}$ has the following form [17]

$$\boldsymbol{H} = \begin{bmatrix} \frac{\boldsymbol{x}_u - \boldsymbol{s}_2}{\|\boldsymbol{x}_u - \boldsymbol{s}_2\|} - \frac{\boldsymbol{x}_u - \boldsymbol{s}_1}{\|\boldsymbol{x}_u - \boldsymbol{s}_1\|} \\ \frac{\boldsymbol{x}_u - \boldsymbol{s}_3}{\|\boldsymbol{x}_u - \boldsymbol{s}_3\|} - \frac{\boldsymbol{x}_u - \boldsymbol{s}_1}{\|\boldsymbol{x}_u - \boldsymbol{s}_1\|} \\ \vdots \\ \frac{\boldsymbol{x}_u - \boldsymbol{s}_m}{\|\boldsymbol{x}_u - \boldsymbol{s}_m\|} - \frac{\boldsymbol{x}_u - \boldsymbol{s}_1}{\|\boldsymbol{x}_u - \boldsymbol{s}_1\|} \end{bmatrix} \quad (18)$$

Then, $\tilde{\boldsymbol{x}}$ is updated by subtracting the estimate of $\delta\hat{\boldsymbol{x}}_u$ from its initial value. Eq. (17) is iteratively solved until $\|\delta\hat{\boldsymbol{x}}_u\|$ is insignificant. Using this result, the position variance of a user can be expressed as

$$\sigma^2_{\boldsymbol{x}_u} = \text{trace}(H^\top W H)^{-1} \quad (19)$$

Eq. (19) is used to compute the theoretical user positioning accuracy in Section IV.

B. Effects of Disturbances on Aerial Nodes and User Positioning Performance

After forming the AHLoS, the aerial nodes will hold their designated node position until a positioning service is finished. However, holding the aerial nodes at the same position throughout the positioning service period may not be possible due to control errors or external disturbance such as wind or gust. The position deviation of the aerial nodes would not cause a problem if the position measurement rate in the aerial nodes is fast enough to capture and timely broadcast the

TABLE I
SENSOR NODE COORDINATES IN THE SIMULATION

Sensor nodes	Coordinates x (m)	y (m)	z (m)
$\boldsymbol{s}_1$	0	0	0
$\boldsymbol{s}_2$	50.00	0	0
$\boldsymbol{s}_3$	0	50.00	0
$\boldsymbol{s}_4$	50.00	50.00	0
$\boldsymbol{s}_{air,1}$	33.73	40.00	15.43
$\boldsymbol{s}_{air,2}$	16.37	48.97	14.52
$\boldsymbol{s}_{air,3}$	14.62	32.29	12.59
$\boldsymbol{s}_{air,4}$	-8.94	39.16	15.75
$\boldsymbol{s}_{air,5}$	40.18	19.47	13.85
$\boldsymbol{s}_{air,6}$	16.49	1.83	12.70

deviated aerial node position in the message. The effect on the user positioning is rather caused by the small change of the sensor node geometry in the AHLoS.

The effects from the disturbances would be best assessed by injecting small position deviations to the aerial sensor nodes in simulation. Further, the positioning accuracy of the AHLoS must be evaluated with the disturbances because the AHLoS may often experience the disturbances in a normal operation. The aerial node disturbance and its positioning effects are further discussed in the later sections.

IV. EXPERIMENTAL RESULTS

This section describes our experimental setup and the results of simulation. We used a total of ten sensor nodes as shown in Fig. 3 with the coordinates as listed in Table I. The first four sensor nodes from $\boldsymbol{s}_1$ to $\boldsymbol{s}_4$ are the reference sensor nodes on the ground. The rest of the nodes, from $\boldsymbol{s}_{air,1}$ to $\boldsymbol{s}_{air,6}$, are the aerial nodes. Initially, the aerial nodes are placed on the ground at the coordinates, [-10, -10, 0]. Once deployment begins, they sequentially lift off and navigate to the designated node position while localizing themselves.

The sensor nodes are assumed to use UWB devices. The range limit of today's commercial UWB devices can extend up to a few hundred meters without any blockages and its range accuracy varies from 2 cm to 15 cm [18], [19]. Since we aim to provide position information that is as precise as possible given the latest UWB ranging performance, we modeled the UWB range accuracy of 5 cm (1σ) in Gaussian random distribution that includes possible UWB time synchronization errors between anchors, noise, and multipath. The sharp pulse shape of the UWB signal is able to greatly resolve multipath induced range errors [20]. The UWB anchor coordinate errors are also computed and included in the range measurement errors during the simulation. Also, the degraded user positioning performance with larger range errors will be discussed in the later subsection.

Fig 4. shows the positioning errors on the flight paths while the aerial nodes navigate to their designated positions at the height of 5 m above the ground. The error is in RSS of 3D position errors and the small magnitude of the errors indicates that the aerial nodes successfully reach to the designated positions.

Fig. 5 shows the convergence of the 3D position error variance of the aerial nodes. The successive refinement process

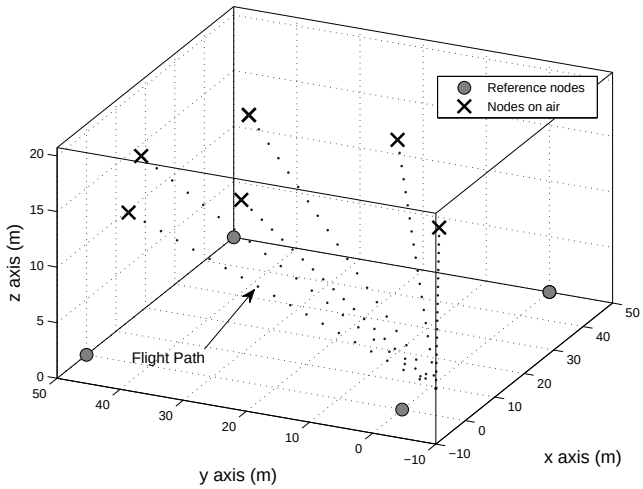

Fig. 3. Geometry of the reference and aerial nodes and the flight path of the aerial nodes during the deployment.

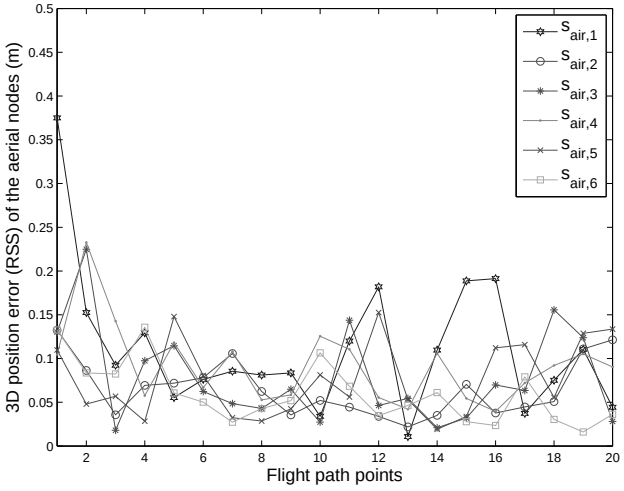

Fig. 4. Position error of the aerial nodes on the 20 flight path points during the initial deployment.

was iterated for 10 times, but the variances quickly converged after the 3^{rd} iteration.

In the sample network geometry given, the user positioning area extends from 5 to 45 m in $\boldsymbol{x}$ axis and 5 to 45 m in $\boldsymbol{y}$ axis. The altitude of a user extends from 0 to 12 m. User positioning errors were evaluated at the total of 16,848 grid points in the defined user positioning space. Fig. 6 shows the standard deviation of the 3D position errors for a user on the ground, while Fig. 7 and Fig. 8 show the standard deviation of the 3D position errors for a user at the altitudes of 6 m and 12 m, respectively. The variance of the 3D position errors tends to increase as the altitude of the user increases in this network geometry. Also note that the user positioning error is consistently large at $x = 45$ m and $y = 0$ m where the user-to-ranging-source geometry is disadvantaged compared to other user locations.

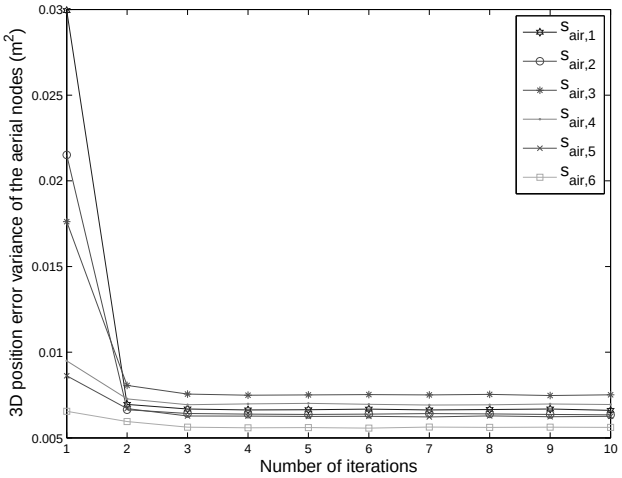

Fig. 5. Position error variance of the aerial sensor nodes.

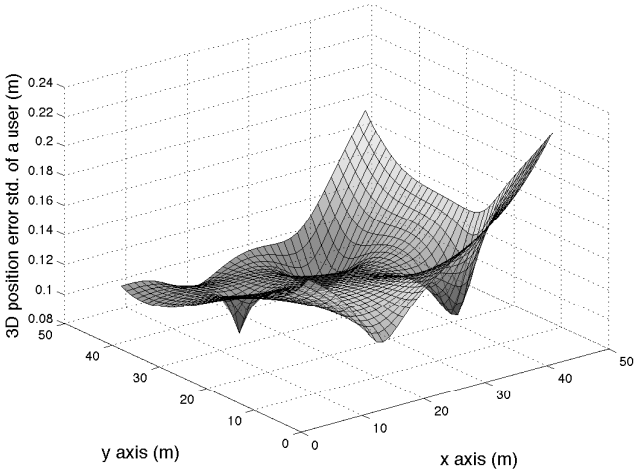

Fig. 8. Position error (1σ) of a user at the height of 12 m.

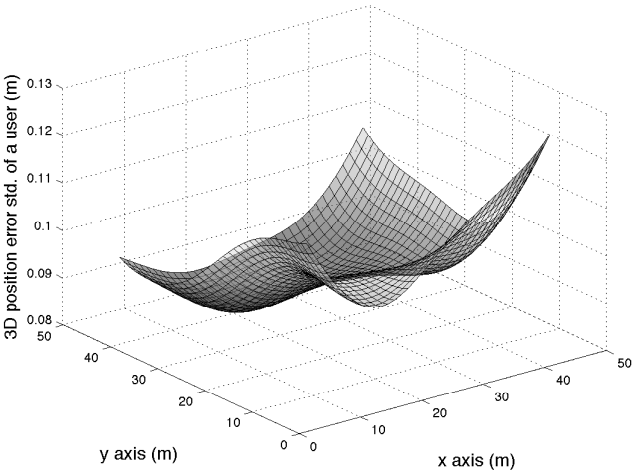

Fig. 6. Position error (1σ) of a user on the ground.

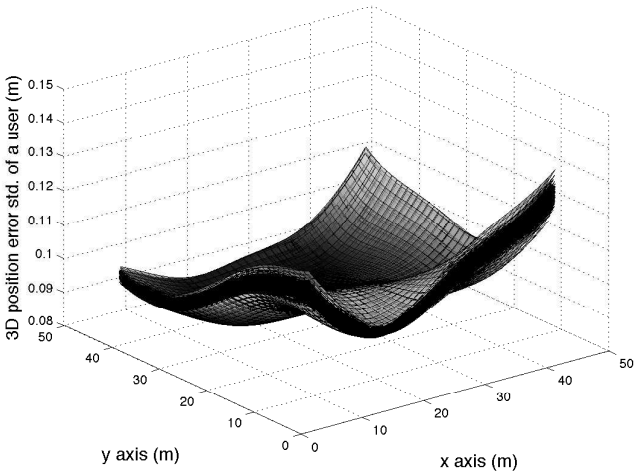

Fig. 9. Position error (1σ) of a user on the ground with aerial nodes disturbance.

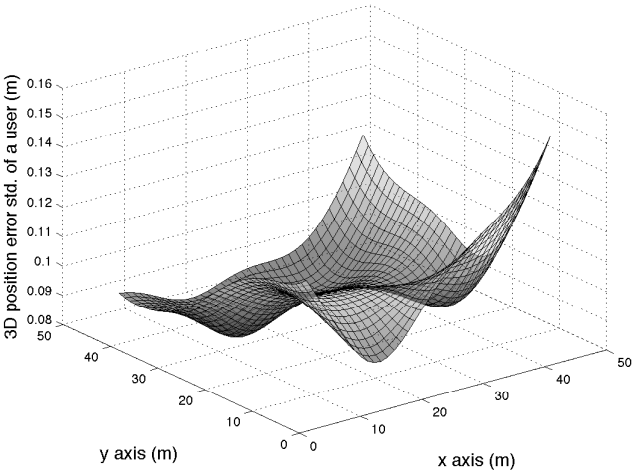

Fig. 7. Position error (1σ) of a user at the height of 6 m.

A. Aerial Node Disturbance Effects on User Positioning Performance

As discussed before, disturbances acting on the aerial nodes will cause slight changes in the network geometry. In this work, the disturbance is modeled as a Gaussian random distribution with zero mean and 50 cm standard deviation in each of the three dimensional axes. A total of 500 different random disturbances are injected into the aerial node positions. Fig. 9, 10, and 11 show the overlapped standard deviation of the 3D position errors in the 500 random cases for the user altitudes at zero, 6, and 12 meters, respectively. Among the figures, the largest variation in the standard deviation occurrs at the altitude of zero and was less than 5 cm.

Fig. 12 and Fig. 13 show the histogram of horizontal and vertical user position errors at the 16,848 grid points given the aerial node diturbances. The horizontal position error distribution has the mean of 0.2 cm and the standard deviation

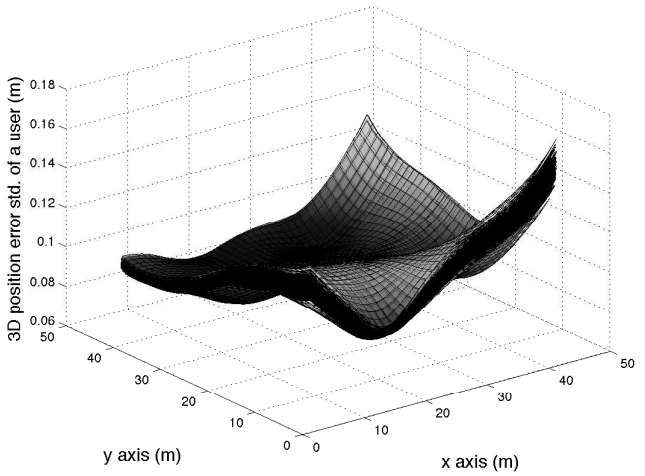

Fig. 10. Position error (1σ) of a user at the height of 6 m with aerial nodes disturbance.

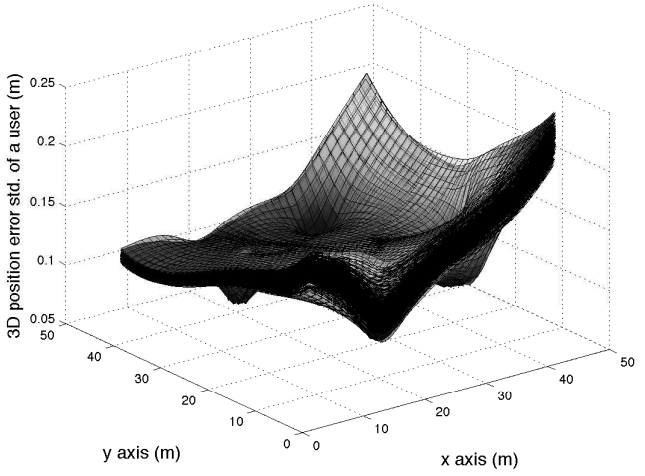

Fig. 11. Position error (1σ) of a user at the height of 12 m with aerial nodes disturbance.

of 4 cm. The vertical position error distribution has the mean of -0.4 cm and the standard deviation of 7 cm.

B. Range Error Sensitivity Analysis

In the above subsections, we assume the ranging accuracy of 5 cm. To see the performance variation of the AHLoS with respect to larger range errors, we injected 10 cm, 15 cm, and 20 cm in the simulation in addition to the disturbance of aerial nodes. The resultant horizontal and vertical position accuracies (1σ) are listed in Table II.

The results in Table II are useful to determine if a particular form of an AHLoS network geometry would also provide a desired positioning accuracy in a dense multipath environment that may degrade an UWB ranging accuracy. If the degradation of the positioning accuracy appears to be significant for a targeted operation, a user could utilize additional onboard sensors, such as a barometric or radar altimeter, to improve the

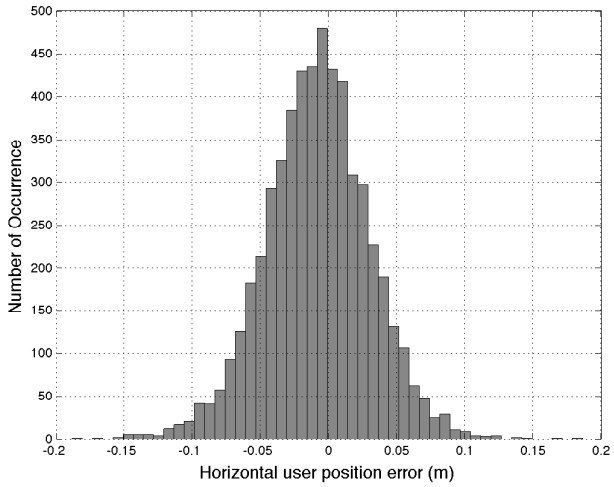

Fig. 12. Histogram of horizontal position error in the user positioning space with aerial nodes disturbance.

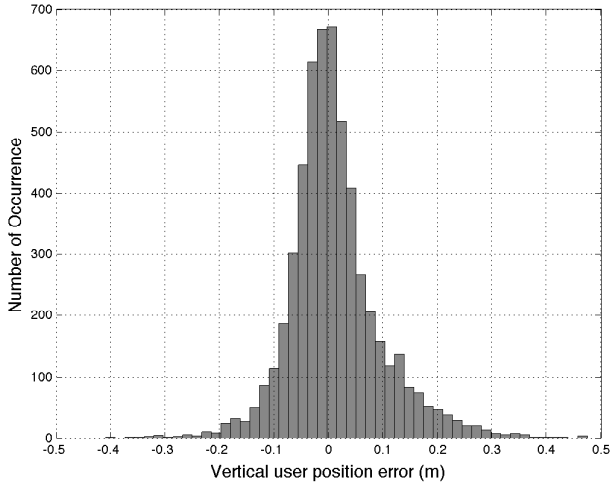

Fig. 13. Histogram of horizontal position error in the user positioning space with aerial nodes disturbance.

TABLE II
HORIZONTAL AND VERTICAL POSITIONING ERROR STANDARD DEVIATION WITH VARIOUS RANGE ACCURACIES

Range accuracy	Horizontal	Vertical
5 cm	4 cm	7 cm
10 cm	7 cm	15 cm
15 cm	11 cm	24 cm
20 cm	15 cm	31 cm

vertical positioning accuracy. Alternatively, a more optimized sensor node geometry can be used.

V. Conclusion

This paper presented a method of 3D Ad Hoc Localization System (AHLoS) that uses UAS in the form of a quadroptor or a similar platform as aerial sensor nodes. We explained the deployment of the 3D AHLoS, localization algorithms, and user positioning error characteristics. We showed that the localization process through successive refinement converges from using the eigenvalue inequalities of the corresponding covariance matrices. We also evaluated the user positioning performance of the 3D AHLoS through a simulation that used ten UWB sensor nodes with various range accuracy and aerial node disturbance. With the range accuracy of 5 cm, the simulation results showed that 1σ of horizontal and vertical user position errors were smaller than 4 cm and 7 cm with negligible biases, respectively. This result suggests that the 3D AHLoS using UWB is suitable for a wide spectrum of applications that require precise vertical positioning. An immediate application we imagine involves an autonomous drone navigation and landing system in GNSS-denied environments. We believe that further optimized node placement in the network will satisfy the required 3D positioning and coverage requirements in those applications.

Acknowledgment

The research presented in this paper was supported in part by the new faculty startup funding from the University of Kansas.

References

[1] S. Tiwari, A. Jain, S. Sarkar, S. Jain, and A. Gwal, "Ionospheric irregularities at antarctic using gps measurements," *Journal of Earth System Science*, vol. 121, no. 2, pp. 345–353, 2012. [Online]. Available: http://dx.doi.org/10.1007/s12040-012-0168-8

[2] Y. Chen and R. Luo, "Design and implementation of a wifi-based local locating system," in *Portable Information Devices, 2007. PORTABLE07. IEEE International Conference on*, May 2007, pp. 1–5.

[3] M. Rabinowitz and J. Spilker, J.J., "A new positioning system using television synchronization signals," *Broadcasting, IEEE Transactions on*, vol. 51, no. 1, pp. 51–61, March 2005.

[4] R. Kshetrimayum, "An introduction to uwb communication systems," *Potentials, IEEE*, vol. 28, no. 2, pp. 9–13, March 2009.

[5] A. Savvides, C.-C. Han, and M. B. Strivastava, "Dynamic fine-grained localization in ad-hoc networks of sensors," in *Proceedings of the 7th annual international conference on Mobile computing and networking*. ACM, 2001, pp. 166–179.

[6] C. Savarese, J. M. Rabaey, and J. Beutel, "Location in distributed ad-hoc wireless sensor networks," in *Acoustics, Speech, and Signal Processing, 2001. Proceedings.(ICASSP'01). 2001 IEEE International Conference on*, vol. 4. IEEE, 2001, pp. 2037–2040.

[7] D. Niculescu and B. Nath, "Ad hoc positioning system (aps) using aoa," in *INFOCOM 2003. Twenty-Second Annual Joint Conference of the IEEE Computer and Communications. IEEE Societies*, vol. 3. IEEE, 2003, pp. 1734–1743.

[8] L. Doherty, L. El Ghaoui *et al.*, "Convex position estimation in wireless sensor networks," in *INFOCOM 2001. Twentieth Annual Joint Conference of the IEEE Computer and Communications Societies. Proceedings. IEEE*, vol. 3. IEEE, 2001, pp. 1655–1663.

[9] P. Biswas and Y. Ye, "Semidefinite programming for ad hoc wireless sensor network localization," in *Proceedings of the 3rd international symposium on Information processing in sensor networks*. ACM, 2004, pp. 46–54.

[10] S. Kim, M. Kojima, H. Waki, and M. Yamashita, "Algorithm 920: Sfsdp: a sparse version of full semidefinite programming relaxation for sensor network localization problems," *ACM Transactions on Mathematical Software (TOMS)*, vol. 38, no. 4, p. 27, 2012.

[11] S. Capkun, M. Hamdi, and J.-P. Hubaux, "Gps-free positioning in mobile ad-hoc networks," in *System Sciences, 2001. Proceedings of the 34th Annual Hawaii International Conference on*, Jan 2001, pp. 1–10.

[12] R. Nagpal, H. Shrobe, and J. Bachrach, "Organizing a global coordinate system from local information on an ad hoc sensor network," in *Information Processing in Sensor Networks*. Springer, 2003, pp. 333–348.

[13] N. Patwari, J. Ash, S. Kyperountas, A. Hero, R. Moses, and N. Correal, "Locating the nodes: cooperative localization in wireless sensor networks," *Signal Processing Magazine, IEEE*, vol. 22, no. 4, pp. 54–69, July 2005.

[14] E. D. Kaplan and C. J. Hegarty, *Understanding GPS: principles and applications*. Artech house, 2005.

[15] G. A. Seber, *A matrix handbook for statisticians*. John Wiley & Sons, 2008, vol. 15.

[16] B. Hu and N. C. Beaulieu, "Accurate performance evaluation of time-hopping and direct-sequence uwb systems in multi-user interference," *Communications, IEEE Transactions on*, vol. 53, no. 6, pp. 1053–1062, 2005.

[17] J. Bard and F. Ham, "Time difference of arrival dilution of precision and applications," *Signal Processing, IEEE Transactions on*, vol. 47, no. 2, pp. 521–523, Feb 1999.

[18] M. Yavari and B. G. Nickerson, "Ultra wideband wireless positioning systems," University of New Brunswick, Fredericton, Canada, Tech. Rep. TR14-230, 2014.

[19] G. Bellusci, G. Janssen, J. Yan, and C. Tiberius, "Model of distance and bandwidth dependency of toa-based uwb ranging error," in *Ultra-Wideband, 2008. ICUWB 2008. IEEE International Conference on*, vol. 3, Sept 2008, pp. 193–196.

[20] D. Dardari, A. Conti, U. Ferner, A. Giorgetti, and M. Z. Win, "Ranging with ultrawide bandwidth signals in multipath environments," *Proceedings of the IEEE*, vol. 97, no. 2, pp. 404–426, 2009.

PLACE PHOTO HERE

Euiho Kim Dr. Euiho Kim is currently with the Department of Aerospace Engineering at the University of Kansas as a research associate. His current research areas are satellite based navigation, aircraft navigation using ground nav-aids, indoor navigation, and robotics. He was the technical lead of the Ground-Based Augmentation System (GBAS) of GPS and FAA's Alternative Position, Navigation, and Timing (APNT) programs when he worked in industry. Dr. Kim completed his Ph.D. and Masters degree in the department of Aeronautics and Astronautics at Stanford University. He finished his undergraduate degree in the department of Aerospace engineering at Iowa State University.

PLACE PHOTO HERE

Dongkyu Choi Dr. Dongkyu Choi is an Assistant Professor in the Department of Aerospace Engineering at the University of Kansas. His research interests include cognitively-inspired control systems, artificial intelligence, and robotics. He has been actively working on autonomous unmanned vehicles for both indoor and outdoor applications with the focus on higher-level control capabilities. Dr. Choi received his MS and PhD in Aeronautics and Astronautics from Stanford University and his BS in Aerospace Engineering from Seoul National University.